CHARACTERIZATION OF 81P/WILD 2 PARTICLES C2067,1,111,6.0 and C2067,1,111,8.0. T. Smith[1], H. Khodja[1], C. Raepsaet[1], M. J. Burchell[2], G. J. Flynn[3], G. F. Herzog[4], J. Park[4], F. Lindsay[4], K. Nakamura-Messenger[5], L. P. Keller[5], S. Taylor[6], and A. Westphal[7] [1] Laboratoire d'Etude des Eléments Légers, UMR 3299 CEA-CNRS-IRAMIS, Gif-sur-Yvette, France (thomas.smith@cea.fr), [2] U. Kent, Canterbury, Kent, CT2 7NH, UK [3] SUNY-Plattsburgh, Plattsburgh NY 12901-2681, [4] Rutgers U., Piscataway, NJ 08854-8087, [5] ARES, NASA Johnson Space Center, Houston, TX 77058, [6] CRREL, 72 Lyme Road, Hanover, NH 03755, [7] SSL, U. California, Berkeley, 94720.

Introduction: The concentrations of C and N in cometary particles are of interest in characterizing the regions where comets formed. One aim of this work is to analyze enough Stardust particles to draw meaningful statistical conclusions about their inventories of C and N. Toward that end we report recent studies of Stardust particles and related materials.

Experimental methods: Table 1 lists the samples studied and the analyses done. Three particles C2067.1.111.6.0, 7.0, and 8.0 (henceforth C6.0, C7.0 and C8.0) were extracted from aerogel and placed on diamond plates for FTIR analyses. Following the FTIR analyses, the particles were embedded in sulfur, and partly microtomed into several slices roughly ~70 nm thick, and then floated these slices onto molybdenum TEM grids with Si/SiO membrane backings and supplied by ESPI. The backings provided physical support for the particles and were thought to be thin enough not to add too much to the Si and O already present in the samples. Additional sections were placed

Table 1.		
Sample	Form	Analyses
C2067.1.111.6.0	in In	NRA, EDX, FTIR, TEM
C2067.1.111.6.12	TEM-Mo	
C2067.1.111.8.0	in In	NRA, EDX, FTIR, TEM
C2067.1.111.8.4	TEM-Mo	
C2067.1.111.7.1	TEM-Mo	NRA
C2067.1.111.7.8	TEM-Mo	
KOCN shot into aerogel	keystone	NRA
Glycine shot into Al	Al	NRA

on carbon film substrates for TEM analyses. After microtomy, the sulfur was sublimed and the remaining portions of the particles were pressed into high-purity indium foil for nuclear reaction analyses (NRA). To reduce NRA backgrounds, each TEM grid was mounted across the mouth of a small well drilled into an Al disk and lined with In foil.

Reports that C and N survive in craters that Stardust particles made in Al on the spacecraft [1-2] encouraged us to attempt quantitative nuclear reaction analyses of residues of the amino acid glycine (NH_2CH_2COOH) shot into Al plates ~102 µm thick.

Finally, [3] reported that analyses of reagent-grade KOCN and NaOCN by the NRA method when calibrated with SiO_2 gave oxygen fractions ~25% higher than expected [3]. They speculated that the nuclear cross section adopted for the reaction $^{16}O(d,p_0)^{17}O$ in reducing the data might have been responsible for the difference. To test this hypothesis, we varied the proton-detection angle from 170°, the one at which we and [3] made measurements, to

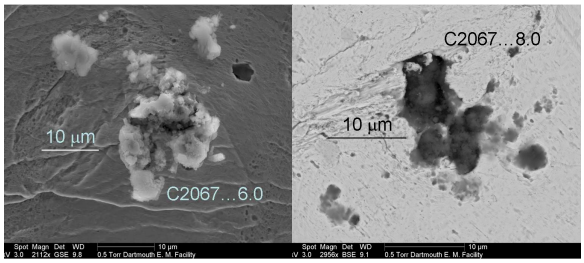

Figure 1. SEM images of C6.0 and C8.0

164.25°, the angle at which the $^{16}O(d,p_0)^{17}O$ nuclear cross section had been measured.

Results: *Stardust fragments* - Figure 1 shows SEM/EDAX images taken of C6.0 and C8.0 without carbon coating. The fragments are ~10 µm across. Signals from Si and O derived from aerogel and the background from the indium foil dominate the EDX spectra of both particles. We saw small signals due to C, Mg, and Fe for C6.0 and due to Mg, S, and Fe for C8.0.

FTIR – Spectra for C6.0, C7.0 and C8.0 were obtained with the extracted particles placed on diamond substrates. The spectra are dominated by Si-O stretching features that are consistent with aerogel mixed with amorphous Mg-silicate. C6.0 shows weak features in the 3.4-µm region that are consistent with aliphatic C-H in hydrocarbons; these features are also present in the spectra from C7.0, but are weaker; we see no aliphatic C-H in particle C8.0. More quantitative analysis is difficult for whole particles as variable sample thickness complicates the interpretation of band depth ratios.

TEM - TEM imaging and chemical mapping data for C6.0 and C8.0 show that both particles are mixtures of compressed aerogel and melt glass. Elemental maps have no C-rich hotspots. Vesicular melt glass that is compositionally heterogeneous with respect to Mg/Si ratio dominates in C6.0. The melt glass contains abundant nanophase Fe metal and sulfide inclusions. Some of the sulfide inclusions are Ni-rich. Particle C8.0 also contains abundandant vesicular melt glass

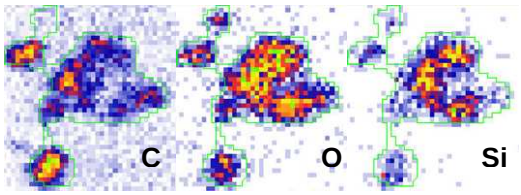

Figure 2. Stardust particle C6.0. Sample outlined in green

with heterogeneous Mg/Si ratios and nanophase Fe metal inclusions; Fe-sulfide grains are rare.

Nuclear reaction analyses – In order to improve data-reduction methods, we first re-analyzed several well-characterized samples under the same experimental conditions used previously. From the results, the detector solid angle was estimated to be 110 msr, a value consistent with an independent Monte-Carlo evaluation. When comparing experimental spectra with simulations based on known compositions, we observed good agreement for C and N with vitreous carbon, KOCN and $K_3Fe(CN)_6$ targets. Some discrepancies on O appear with SiO_2, Al_2O_3 and glycine. For quartz and alumina, changing the detection angle from 170° to 164.25°, improved the agreement, at least for the high energy part of the spectrum. In particular, the simulated-to-experimental, integrated count ratio increased from 0.95 at 170° to 0.99 at 164.25°, which we consider satisfactory. For glycine, we speculate that the observed differences could be explained by large losses of H and CO due to the interactions with the incoming beam.

The areal densities and their Poisson errors for Si, O, C and N of several samples are given in Table 2. To correct for instrumental blanks and possible mounting blanks, map data (e.g., Figure 2) were divided in two parts, one containing the sample itself, and the second all the rest. Comparisons were made between the number of counts for each element in the "sample zone" and in the "blank zone". The difference gives the effective number of counts to be simulated using SIMNRA program [4].

Oxygen and silicon dominate the elemental compositions of Stardust particles C6.0, C6.12 and C7.0, as in C23 and C41 in [3] and C21 in [5]. The Si/O atom ratio for particle C6.0 is close to the expected value of 0.5 for silica. For particle C8.0 the ratio is 0.39 which is about 20% lower than silica ratio. The observed Si/O ratios are consistent with the presence of aerogel mixed with some cometary material and affirm the SEM and FTIR measurements. Removal of the aerogel blank from the Stardust signal is calculated using the same procedure as described in [3] and [5]. It appears that for particle C8.0, most of the C concentration derives from aerogel. Nitrogen abundances are low for samples C6.0, C8.0 and C6.12, as in C2103 and C2065 in [5]. In Stardust TEM C2067.1.111.7.1, the atom fraction of nitrogen is higher and represents 10.7%.

The calculated C/N ratios increase from 3.3 in particles C6.1 and C7.12 to 43.6 in C6.0 whereas previous data obtained by [3] varied from 11 to 51 and from 8 to 14 in [6]. As a comparison, the C/N ratios are about 12.6 for CI chondrites and 20 for comets [3]. Great lability for N than for C [3] during impact with aerogel may have caused preferentially a loss of N on capture. If so, our calculated C/N ratios would be higher than those of the cometary particles before impact.

Glycine craters – Glycine samples were shot into aluminum foils at 6.34 km/s so as to simulate the conditions occurring during Wild 2 particle capture. Information on dust velocity and density can be derived from these experiments [7]. We were able to process the data on one of the three examined samples, G150310. Results are given in Table 2. The C/N and O/C ratios are respectively 7.1 and 3.2 instead of 2.0 expected from stoichiometry. These results indicate loss of light elements, even larger than for the glycine reference, probably due to the impact itself.

References: [1] Stadermann F. J. et al. (2008) *M&PS*, *43*, 299-313. **[2]** Kearsley A.T. et al. (2010) *LPSC*, 41, abstract #1971. **[3]** Gallien J-P. et al. (2008) *M&PS*, *43*, 335-351. **[4]** Mayer M. (1997) *Report IPP 9/113*. **[5]** Khodja H. et al. (2009) *LPSC*, 40, abstract #1746. **[6]** Cody G. et al. (2008) *M&PS*, *4*, 353-365. **[7]** Kearsley A.T. et al. (2008) *M&PS*, *43*, 41-73.

Table 2. Atomic areal density (10^{15} atom/cm^2) by NRA.

		Si	O	C	N
C6.0	a	1139-26	15.7-0.8	25.2-4.7	59-12
	b	1317	2815	905	13
	c	0	182±2	558±6	13±3
C8.0	a	1473-96	23.4-1.8	9.86-5.97	44-32
	b	1024	2613	101	2
	c	0	565±5	0	2±2
C7.1	a	124-137	4.81-1.96	17.1-4.3	601-9
	b	86	599	478	140
	c	0	428±17	456±7	140±7
C6.12	a	179-156	2.40-1.10	5.92-4.30	77-12
	b	36	273	59	15
	c	0	201±13	50±4	15±3
G150310	a		19.8-0.9	22.8-9.03	397-81
	b	0	5004±107	1544±27	218±20

a) Counts –background; O and C ($\times 10^3$). b) Areal density ($\times 10^{15}$ at/cm^2). c) Areal density less aerogel contribution ($\times 10^{15}$ at/cm^2).